Conformal Perfectly Matched Layers for the Time Domain Finite Element Method

Thomas Rylander* and Jian-Ming Jin
Center for Computational Electromagnetics
Department of Electrical and Computer Engineering
University of Illinois at Urbana-Champaign
Urbana, Illinois 61801-2991

1 Introduction

The perfectly matched layer (PML) is very popular and efficient for grid truncation of open-region problems. The concept of PML was introduced by Bérenger [1] together with a numerical implementation based on the finite-difference time-domain (FDTD) scheme. However, the basic FDTD scheme is formulated on Cartesian grids and in many cases an unnecessarily large free-space region must be discretized between the PML and the object under investigation.

The PML has been formulated in cylindrical and spherical coordinate systems by Teixeira and Chew [2] in order to reduce the free space region for objects that conform well to circular cylinders and spheres. A more attractive setting would, of course, not rely on a specific coordinate system. Recently, Teixeira et al. [3] developed a conformal PML for the FDTD scheme. Here, we continue this effort by presenting a new conformal PML formulation for the finite element method (FEM) in the time domain. It is based on the anisotropic material [4] which has been used for the time domain FEM by Jiao et al. [5].

In this paper, we present the 2D-version of the conformal PML, which is a special case of our 3D-formulation. Furthermore, we consider only radar cross section (RCS) computations based on the scattered field formulation and emphasize that our PML is applicable to the total field formulation as well as radiating structures.

2 Formulation

We enclose the boundary Γ_0 of the scatterer by a conformal and convex boundary Γ_{PML} as shown in Fig. 1(a). The region Ω_0 (bounded by Γ_0 and Γ_{PML}) is then discretized by triangles. A typical discretization for a circular cylinder is shown in Fig. 1(b). Given the triangulation, we construct a grid of quadrilaterals by extruding the line segments on Γ_{PML} in the outward normal direction from Ω_0.

Our conformal PML formulation for the FEM in the time domain is based on

$$\nabla \times \vec{\vec{\mu}}_r^{-1} \nabla \times \vec{E} - k_0^2 \vec{\vec{\epsilon}}_r \vec{E} = \vec{0} \tag{1}$$

0-7803-7846-6/03/$17.00 ©2003 IEEE

with appropriate boundary conditions. We use $\vec{\vec{\mu}}_r = \mu_r \vec{\vec{\Lambda}}$ and $\vec{\vec{\epsilon}}_r = \epsilon_r \vec{\vec{\Lambda}}$, where

$$\vec{\vec{\Lambda}} = \hat{u}\frac{1}{\gamma_u}\hat{u} + \hat{v}\gamma_u\hat{v} + \hat{w}\gamma_u\hat{w} \tag{2}$$

and $\gamma_u = 1 + \sigma/j\omega\epsilon_0$. The conductivity σ controls the attenuation rate of the electromagnetic fields in the $\hat{u}$-direction, where $\hat{u}$ is defined at each node and aligned with the edges which are normal to Γ_{PML}. Similarly, $\hat{v} = \hat{z} \times \hat{u}$ is defined at each node and we fix $\hat{w} = \hat{z}$. The conductivity σ is set to zero for all triangles and consequently Eq. (2) gives the unity tensor in Ω_0, regardless the choice of $\hat{u}$. We use linear interpolation to evaluate $\hat{u}$ and $\hat{v}$ inside each element.

The electric field is expanded in terms of linear edge elements and we use Galerkin's method to deduce the weak form of Eq. (1), where its time domain counterpart is obtained by the Fourier transform. Similarly, the time dependence of the electric field is expressed as a piecewise linear function and, again, we exploit the Galerkin's method. The Newmark scheme is used for the time integration and we derive it by forming the linear combination of trapezoidal and exact integration applied to the temporal part of the weak form. The convolutions of the type $\int_0^t ae^{-b\,(t-\tau)} f_j(\tau)d\tau$ are evaluated recursively by

$$\psi_j(\vec{r}, t) = e^{-b\,(t-t_1)}\psi_j(\vec{r}, t_1) + ae^{-b\,t}\int_{t_1}^{t} e^{b\tau} f_j(\tau)d\tau, \tag{3}$$

where a and b, in general, depend on $\vec{r}$. In Eq. (3), $f_j(\tau)$ is either $E_j(\tau)$ or $\partial_\tau E_j(\tau)$.

3 Numerical examples

In this paper, we present initial tests of the new PML formulation for scattering from a perfect electric conductor (PEC) circular cylinder with the radius 0.5 m. A typical discretization is shown in Fig. 1(b). The amplitude of the incident plane wave is given from

$$E_i(t) = E_0 \exp\left[-\left(\frac{t-t_0}{d_0}\right)^2\right]\sin\left[\omega_0(t-t_0)\right], \tag{4}$$

which provides a localized pulse in both time and frequency domain. We impose the boundary condition $\hat{n} \times \vec{E}_s = -\hat{n} \times \vec{E}_i$ on the surface Γ_0 of the scatterer and solve for the scattered field $\vec{E}_s$. The PML is backed by the boundary condition $\hat{n} \times \vec{E}_s = \vec{0}$ and we use a quadratic profile $\sigma(\rho) = \sigma_m(\rho/\delta)^2$, where ρ is the distance from Γ_{PML} and δ is the thickness of the PML. The RCS is computed from

$$\sigma_{\mathrm{2D}}(\hat{r}_c) = \lim_{r_c\to\infty} 2\pi r_c \frac{|\vec{E}_s|^2}{|\vec{E}_i|^2} = \frac{k}{4|\vec{E}_i|^2}\left(|L_z + ZN_\phi|^2 + |L_\phi - ZN_z|^2\right), \tag{5}$$

where the scattering amplitudes are given from

$$\vec{N}(\hat{r}_c) \;=\; \oint_{\Gamma_{\mathrm{NTF}}} \vec{J}_s(\vec{r}_c^{\,\prime})e^{+jk\hat{r}_c\cdot\vec{r}_c^{\,\prime}}dL', \quad \text{and} \tag{6}$$

$$\vec{L}(\hat{r}_c) \;=\; \oint_{\Gamma_{\mathrm{NTF}}} \vec{M}_s(\vec{r}_c^{\,\prime})e^{+jk\hat{r}_c\cdot\vec{r}_c^{\,\prime}}dL'. \tag{7}$$

The boundary $\Gamma_{\rm NTF}$ is indicated by the thick dashed line in Fig. 1(b). In Eq. (6) and Eq. (7), we have $\vec{J}_s = \hat{n} \times \vec{H}$ and $\vec{M}_s = -\hat{n} \times \vec{E}$.

Figure 2 shows the RCS for the frequencies $f = 0.4$, 0.58, 0.75, and 0.92 GHz given the solution from a single time domain computation. Here, we choose $\Gamma_{\rm NTF}$ and $\Gamma_{\rm PML}$ to be (concentric) circles with the radii 0.6 m and 0.9 m, respectively. The thickness δ of the PML region is 0.43 m and it is discretized (radially) by 16 quadrilaterals. We use a quadratic profile with $\sigma_m \Delta t/\epsilon_0 = 0.35$. The typical cell size is $h = 0.027$ m which gives $\lambda/h = 28.3$, 19.5, 15.1, and 12.3 for the results shown in Fig. 2.

We use the preconditioned conjugate gradient method to solve the linear system of equations for each time step. The residual is reduced a factor 10^{-14} within roughly 10-15 iterations when we use an incomplete LU-decomposition with zero fill-in as a preconditioner. This is a promising result which indicates that the new conformal PML algorithm for the time domain FEM can yield efficient computations.

Empirically, our new conformal PML formulation for the time domain FEM shows stable time stepping for all cases that we have analyzed so far. Other ways to discretize the temporal part of the strong form have shown late time instabilities. We are currently working toward a proof of stability for our conformal PML formulation.

References

[1] J. P. Bérenger, "A perfectly matched layer for the absorption of electromagnetic waves," *J. Comput. Phys.*, vol. 114, pp. 185–200, October 1994.

[2] F. L. Teixeira and W. C. Chew, "Systematic derivation of anisotropic PML absorbing media in cylindrical and spherical coordinates," *IEEE Microw. Guided Wave Lett.*, vol. 7, pp. 371–373, November 1997.

[3] F. L. Teixeira, K. P. Hwang, W. C. Chew, and J. M. Jin, "Conformal PML-FDTD schemes for electromagnetic field simulations: A dynamic stability study," *IEEE Trans. Antennas Propagat.*, vol. 49, pp. 902–907, June 2001.

[4] Z. S. Sacks, D. M. Kingsland, R. Lee, and J. F. Lee, "A perfectly matched anisotropic absorber for use as an absorbing boundary condition," *IEEE Trans. Antennas Propagat.*, vol. 43, pp. 1460–1463, December 1995.

[5] D. Jiao, J. M. Jin, E. Michielssen, and D. Riley, "Time-domain finite-element simulation of three-dimensional scattering and radiation problems using perfectly matched layers," *IEEE Antennas and Propagation Society International Symposium*, vol. 2, pp. 158–161, 2002.

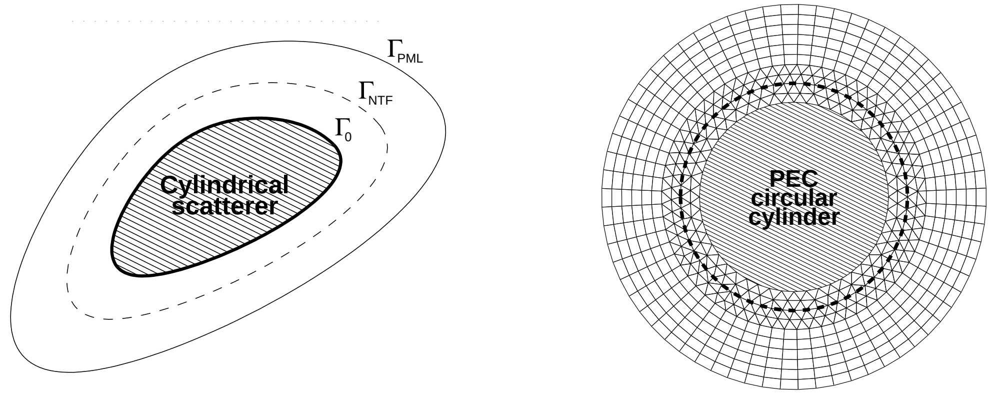

(a) (b)

Figure 1: (a) Labeling of boundaries. (b) Typical discretization shown for a circular cylinder.

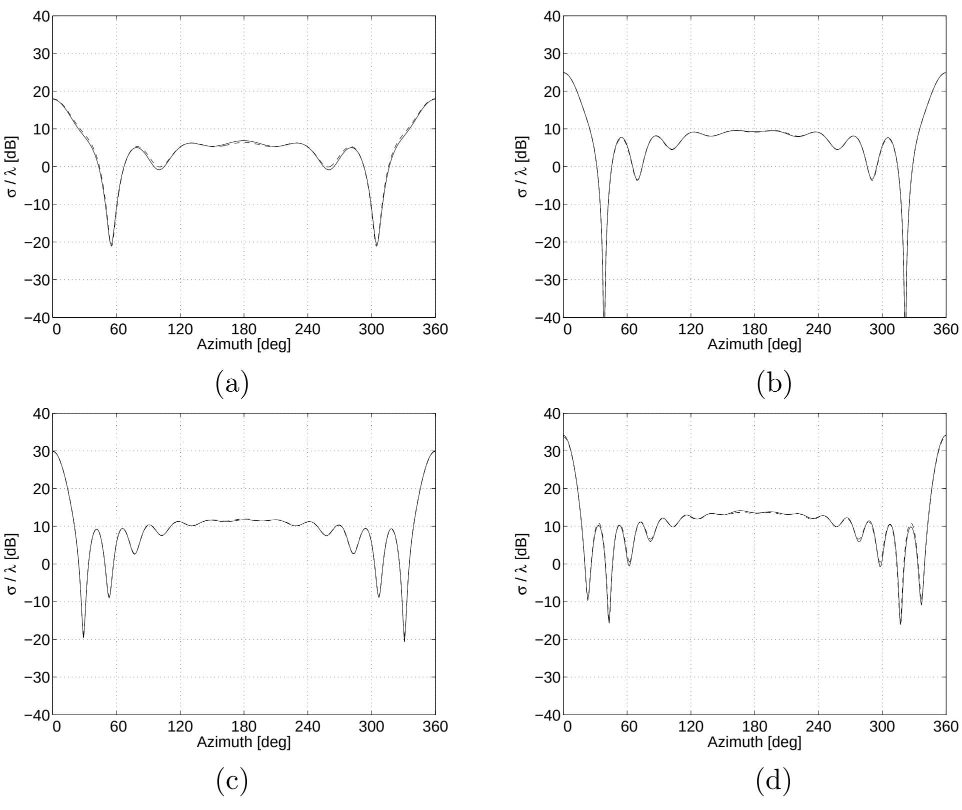

Figure 2: The computed RCS is shown by solid curves and the analytical RCS by the dashed curves for (a) $f = 0.40$ GHz, (b) $f = 0.58$ GHz, (c) $f = 0.75$ GHz, and (d) $f = 0.92$ GHz.